Listeria Protein ActA Mimics WASP Family Proteins: It Activates Filament Barbed End Branching by Arp2/3 Complex

Rajaa Boujemaa-Paterski,[‡,§] Edith Gouin,[§,||] Guido Hansen,[⊥] Stanislav Samarin,[‡] Christophe Le Clainche,[‡] Dominique Didry,[‡] Pierre Dehoux,[||] Pascale Cossart,[||] Christine Kocks,[⊥] Marie-France Carlier,*[,‡] and Dominique Pantaloni[‡]

Dynamique du Cytosquelette, LEBS, CNRS, 91198 Gif-sur Yvette, France, Interaction Bactéries-Cellules, Institut Pasteur, 75724 Paris, France, and Institut für Genetik, University of Cologne, Germany

Received March 9, 2001; Revised Manuscript Received May 29, 2001

ABSTRACT: Actin-based propulsion of the bacteria *Listeria* and *Shigella* mimics the forward movement of the leading edge of motile cells. While *Shigella* harnesses the eukaryotic protein N-WASp to stimulate actin polymerization and filament branching through Arp2/3 complex, the *Listeria* surface protein ActA directly activates Arp2/3 complex by an unknown mechanism. Here we show that the N-terminal domain of ActA binds one actin monomer, in a profilin-like fashion, and Arp2/3 complex and mimics the C-terminal domain of WASp family proteins in catalyzing filament barbed end branching by Arp2/3 complex. No evidence is found for side branching of filaments by ActA-activated Arp2/3 complex. Mutations in the conserved acidic ^{41}DEWEEE^{46} and basic ^{146}KKRRK^{150} regions of ActA affect Arp2/3 binding but not G-actin binding. The motility properties of wild-type and mutated *Listeria* strains in living cells and in the medium reconstituted from pure proteins confirm the conclusions of biochemical experiments. Filament branching is followed by rapid debranching. Debranching is 3−4-fold faster when Arp2/3 is activated by ActA than by the C-terminal domain of N-WASp. VASP is required for efficient propulsion of ActA-coated beads in the reconstituted motility medium, but it does not affect the rates of barbed end branching/debranching by ActA-activated Arp2/3 nor the capping of filaments. VASP therefore affects another still unidentified biochemical reaction that plays an important role in actin-based movement.

The spatial control of actin assembly in response to signaling is an essential feature of actin-based motility. The intracellular pathogens *Listeria*, *Shigella*, and the vaccinia virus, which undergo actin-based propulsion in the host cytoplasm, are acknowledged models for the leading edge of motile cells (*1*−*3* for reviews). *Listeria* has been instrumental in identifying the Arp2/3 complex (a seven polypeptide complex comprising actin-related proteins Arp2 and Arp3) as the cellular factor responsible for stimulating actin polymerization at the bacterial surface (*4*). This function requires the interaction of Arp2/3 complex with the *Listeria* surface protein ActA (*5*). In eukaryotic cells, the Arp2/3 complex is involved in a large variety of motility processes (*6*−*13*). Its function requires its interaction with proteins of the Scar/WASp[1] family (*14*, *15*). The ubiquitous N-WASp protein is harnessed by *Shigella* (*16*) and the vaccinia virus (*17*) to recruit Arp2/3 complex and stimulate actin assembly.

WASp proteins are multidomain connectors which are maintained in an inactive conformation by an internal contact (*18*, *19*). They contain a cryptic "catalytic" C-terminal domain (called VCA, for verprolin homology, cofilin homology and acidic, from the N- to the C-terminal end) that interacts with G-actin and Arp2/3 complex and several "regulatory" domains that bind signaling effectors such as PIP2, the small G-protein Cdc42-GTP, the adaptor Grb2, or the *Shigella* surface protein IcsA. Binding of these effectors targets WASPs to the membrane and relieves the autoinhibited fold of WASp, thus exposing the active VCA domain to actin and Arp2/3 complex (*8*).

Kinetic studies show that, in the presence of Arp2/3 complex and either the VCA domain of N-WASP, or IcsA and N-WASp, or ActA, actin polymerization is strongly accelerated (*8*, *16*, *20*, *21*). In solutions of actin, VCA, and Arp2/3 complex, branched filaments are formed (*22*), which have the same morphology as the dendritic filament array in the lamellipodia (*7*). Analysis of the autocatalytic polymerization curves and EM observations of the length correlation and length ratio of the mother and daughter branches indicated that filaments are multiplied by barbed

[†] M.-F. C. ackonwledges financial support from the Ligue Nationale contre le Cancer, and a grant from Human Frontiers in Science no. RG 0227/1998. C.K. acknowledges financial support from the Deutsche Forschungsgemeinschaft through SFB 274.

* To whom correspondence should be addressed. E-mail: carlier@lebs.cnrs-gif.fr. Phone: (33) 01 69 82 34 65. Fax: (33) 01 69 82 31 29.

[‡] Dynamique du Cytosquelette.

[§] R. B.-P. and E. G. equally contributed to this work.

[||] Interaction Bactéries-Cellules.

[⊥] Institut für Genetik.

[1] Abbreviations: WASp, Wiskott-Aldrich Syndrome protein; N-WASp, neural WASp; Scar, Suppressor of cyclic-AMP receptor; VCA, verprolin homology, cofilin homology, acidic region; VASP, vasodilator-stimulated phosphoprotein; EVH1, Ena-VASP homology domain 1; PIP2, phosphatidylinositol 4,5 diphosphate; HEPES, *N*-(2-hydroxyethyl)piperazine-*N*′-(2-ethane sulfonic acid).

10.1021/bi010486b CCC: $20.00
Published on Web 08/30/2001

end branching (*23*). In contrast, recent fluorescence video-microscopy observations of actin polymerized in the presence of rhodamine-phalloidin, activated Arp2/3 complex, and Alexa 468-phalloidin-stabilized filaments suggested that Arp2/3 induced filament branching from the sides of existing filaments (*24*). The details of the interactions of Arp2/3 complex, VCA, and G-actin with the filaments that lead to the formation of a branch are not elucidated yet. However, the VCA domain of WASp and N-WASp binds Arp2/3 complex via a "cofilin homology" KRSKA basic region and an acidic DEWED consensus sequence and G-actin via the verprolin homology region (*14*).

N-WASp is sufficient to elicit actin-based movement of *Shigella* (*25*), and N-WASp-coated polystyrene microspheres move rapidly, too (Wiesner and Carlier et al., unpublished material), in a minimum motility medium reconstituted from five pure proteins: actin, Arp2/3 complex, actin depolymerizing factor (ADF/cofilin), a capping protein, and profilin. In contrast, movement of *Listeria* is very inefficient in this medium unless the protein VASP is added. VASP is a member of the Ena/VASP family which localizes at focal adhesions (*26*) and at the leading edge of motile cells (*27*) and whose function is not understood. These facts raise important issues regarding, first, the mechanism by which ActA interacts with Arp2/3 complex, stimulates actin assembly, and elicits bacterial actin-based motility, and second, the role of VASP in each of those reactions.

The interaction of ActA with Arp2/3 complex and actin has been addressed in two recent papers, which come up to different conclusions. Skoble et al. (*28*) delineated three regions in a minimal functional fragment [1−160] of ActA, which were involved in actin-based motility. The N-terminal [31−58] region, which contains the ^{41}DEWEEE^{46} consensus acidic sequence, and the ^{146}KKRRK^{150} cofilin homology basic sequence homologous to the one in VCA were involved in Arp2/3 function, and the central region [60−101] was involved in actin binding, in agreement with previous evidence (*29*, *30*). A different topology of ActA interactions with Arp2/3 and actin was proposed by Zalevsky et al. (*31*). Two regions of ActA ([85−104] and [121−138]) were proposed as verprolin homology regions binding two actin monomers. The Arp2/3 binding site was located in region [144−170] of ActA, C-terminal to the actin binding sites. The homologue of the acidic DEWE region of VCA was proposed to be ^{166}DKPTK^{170}, C-terminal to the cofilin homology region.

To clarify how ActA interacts with Arp2/3 complex and G-actin and to determine whether ActA promotes filament branching by Arp2/3 by the same mechanism as the VCA domain of N-WASp, we have combined mutagenesis, biochemistry and video-microscopy approaches. We examine how the protein VASP affects the filament branching/debranching activity of ActA-Arp2/3 complex in relation with its function in motility of *Listeria* and ActA-coated beads.

EXPERIMENTAL PROCEDURES

Bacterial Strains. The bacterial strains used in this work are Bof 343, *L. monocytogenes* L028 wild-type strain; BUG 1625, *L. monocytogenes* L028 isogenic derivative expressing ActA ^{146}KKRR^{149}-4A; BUG 1710, *L. monocytogenes* L028 isogenic derivative expressing ActA Δ^{41}DEWEEE^{46}; BUG 1786, *L. monocytogenes* L028 isogenic derivative expressing ActA W43A. *L. monocytogenes* strains were grown in brain-heart infusion (BHI) medium.

Antibodies. Anti-ActA antibody A16 recognizes region 50−126 (Gouin et al., unpublished material). Anti-Arp3 antibodies were described earlier (*32*).

PIP2. Liposomes made of 90% phosphatidylcholine and 10% PIP2 (Sigma) were prepared by several freeze and thaw cycles and filtered twice through 0.4 μm nucleopore filters (*33*).

Construction of the L. monocytogenes Mutant Strains. Mutant strains were constructed by allelic exchange after transformation of the *Listeria* wild-type strains L028 (Bof343) with a plasmid carrying a mutated *actA* gene. The *Eco*RI−*Sph*I fragment of plasmid pActA3 (*34*) containing the promoter and a part of the *actA* gene corresponding to the first 164 amino acids of the protein was cloned in a plasmid pUC18. Mutagenesis was performed by using an oligonucleotide-directed mutagenesis system (Chameleon, Stratagene) and the following primers: 5′-CCTCGCTTGGTTGCTCT-TCTGTTTTTGTGTTTAAACTAGAATCTTCGCTATCT-GTCGCTGC-3′ for the construct ActA-Δ41−46, 5′-CTG-TTTTTTCTTCTTCCGCTTCATCTGTGTTTAGAC-3′ for the construct W43 → A, and 5′-TGCTATGGCTTTCGCT-GCAGCTGCAATTTCCGCTGC-3′ for the construct ^{146}KKRR^{149} → AAAA.

Following mutagenesis, the sequence of the entire actA fragment was determined. Recombinant plasmids harboring the desired mutations were digested with *Eco*RI−*Sph*I and cloned into pActA3 to recover an entire actA gene. The 2.8 kb *Eco*RI−*Sal*I fragments recovered from the different pActA3 derivatives were cloned into the shuttle vector pKSV7 (*35*). The pKSV7 derived plasmids were electroporated into *L. monocytogenes* L028 and gene replacement was performed as described (*36*).

Expression and purification of 6xhis-tagged ActA derivatives. The N-terminal regions of the various ActA mutants were produced as 6His-tagged fusion proteins. The corresponding regions were amplified by PCR using as templates the different mutated plasmids and primers (*37*). The amplified fragments were cloned into the *Nco*I and *Hind*III sites of pET28b expression vector (Novagen) and the resulting plasmids were used to transform *E. coli* strain BL21(DE3) for expression of the recombinant proteins. The nucleotide sequences of the amplified fragments were verified by sequencing. Purification of the mutated proteins was carried out as described (*37*).

Soluble His-tagged full-length ActA and ActAΔ70−85 were expressed in *L. monocytogenes* and purified as described (*29*).

Actin and Actin-Binding Proteins. Actin was isolated from rabbit muscle and purified in the CaATP-G-actin form by Sephadex G-200 chromatography in G-buffer (5 mM Tris-Cl^-, pH 7.8, 0.1 mM $CaCl_2$, 0.2 mM ATP, 1 mM DTT, and 0.01% NaN_3). Actin was fluorescently labeled with pyrenyliodoacetamide. CaATP-G-actin was converted into MgATP-G-actin by adding 20 μM $MgCl_2$ and 0.2 mM EGTA to a 10 μM CaATP-G-actin solution in G buffer. Arp2/3 complex was purified from bovine brain (*16*). Recombinant histidine-tagged human VASP was expressed and purified as described previously (*38*). Spectrin-actin seeds were prepared from

human erythrocytes (*39*). Gelsolin was a kind gift from Dr Yukio Doi (University of Kyoto). Proteins used in the reconstituted motility assay (Actin Depolymerizing Factor, capping protein, profilin) were purified as described (*25*).

In Vitro Protein Binding Assay. Twenty microliters of Ni agarose coupled to 1 nmol of His-tagged VASP or 20 μL of Gluthatione Sepharose coupled to 1 nmol of GST-VCA were equilibrated in buffer S (20 mM Tris-Cl^-, pH 7.8, 100 mM KCl, 1 mM $MgCl_2$, 0.2 mM ATP, and 1% BSA). Beads were mixed with various quantities of Arp2/3 in 200 μL of buffer B (20 mM Tris-Cl^-, pH 7.8, 100 mM KCl, 1 mM $MgCl_2$, 0.2 mM ATP, 0.1% Tween 20, and 0.2% BSA) and incubated for 1 h at 4 °C on a rotating wheel. Supernatant were collected and beads were washed twice with buffer B. Free and bound Arp2/3 were detected by Western Blotting using a polyclonal anti-Arp3 antibody.

Polymerization Assays. Actin polymerization was monitored by the increase in fluorescence of 5−10% pyrenyl-labeled actin. Fluorescence measurements were carried out at 20 °C in either a Spex Fluorolog 2 or a Safas flx spectrofluorimeter. It was first verified that binding of ActA to G-actin does not affect the fluorescence of pyrenyl-G-actin. Since ActA does not bind to F-actin (see Results), the increase in pyrenyl-actin fluorescence truly reflects the formation of F-actin. The effect of ActA variants on the stimulation of Arp2/3 branching activity was quantitated as follows. The maximal rate of polymerization V, which is measured at the time of mid-polymerization because of the autocatalytic character of the polymerization process (*23*), is taken as a measure of the number of filament ends generated by branching at $t_{1/2}$, and provides an evaluation of the concentration of activated Arp2/3 complex, i.e., of the saturation of Arp2/3 by ActA and G-actin. The relative increase in maximal rate represents the fraction of Arp2/3 in the active complex. The following equation was used to fit the data, in which $[A_0]$ and $[X_0]$ are the total concentrations of Arp2/3 and ActA, respectively, and K represents the equilibrium dissociation constant for the binding of ActA in the active complex (AX).

$$\frac{V - V_0}{V_\infty - V_0} = \frac{[AX]}{[A_0]} = \frac{[A_0] + [X_0] + K \pm \sqrt{([A_0] + [X_0] + K)^2 - 4[A_0][X_0]}}{2[A_0]} \quad (1)$$

The value of K was adjusted by hand to obtain the best fit to the experimental curves. Note that in the above analysis, the binding of G-actin in the active complex is not explicited and is implicitly considered as saturating. However, the values of K can be compared since all ActA variants were tested at the same concentrations of Arp2/3 complex and G-actin (2.5 μM) and the same value of the maximal rate was obtained with all ActA variants, indicating that the same saturating amount of active complex was formed.

Steady-state measurements of F-actin were carried out after overnight incubation of solutions of F-actin and ActA in the presence or absence of gelsolin as described (*16*). The value of the equilibrium dissociation constant (K') for the ActA-G-actin complex was derived from the linear dependence of the steady-state amount of F-actin on the total concentration of ActA, according to eq 2.

$$K' = C_C^P \cdot \left(\frac{[X_0]}{[F(0)] - [F([X_0])]} - 1 \right) \quad (2)$$

where C_C^P represents the pointed end critical concentration, $[X_0]$ the total concentration of ActA, and $[F(0)]$ and $[F([X_0])]$ the concentrations of F-actin measured in the absence and presence of ActA at the concentration $[X_0]$, respectively.

Initial rates of filament growth at the pointed or barbed end were carried out using either 0.2 nM spectrin-actin seeds (barbed end growth) or 3 nM gelsolin-actin seeds (pointed end growth). Seeds were added at time zero to a solution of 2.5 μM pyrenyl-labeled MgATP-G-actin in F buffer. The value of the equilibrium dissociation constant for the ActA-G-actin complex was derived from the dependence of the rate of pointed end growth on the concentration of ActA, using eq 3, derived as follows.

$$V/V_0 = (C - C_C^P)/(C_0 - C_C^P)$$

$$\frac{V}{V_0} = \frac{1}{C_0 - C_C^P} \cdot \left(\frac{C_0 - [X_0] - K' \pm \sqrt{(C_0 - [X_0] - K')^2 + 4K'C_0}}{2} - C_C^P \right) \quad (3)$$

where V_0 and V are the initial rates of pointed end growth measured in the absence and in the presence respectively of ActA at the total concentration $[X_0]$, C_0 and C are the total and free (non-ActA-bound) concentrations of G-actin and C_C^P the pointed end critical concentration. The value of K' was adjusted by hand to find the best fit to the experimental curves.

Fluorescence Microscopy Visualization of Filaments Polymerized in the Presence of ActA and Arp2/3. The method (*22*) was used, with the following modifications. MgATP-G-actin (5 μM, 10% pyrene labeled) was polymerized for 5 min in the presence of 30 nM Arp2/3 and 0.2 μM ActA, with or without VASP (0.2 μM). A pyrene fluorescence polymerization assay of the sample first showed that at time 5 min at least 90% of the polymerization was reached. The addition of 1 M equiv to actin of rhodamine phalloidin at time 5 min, therefore, only stabilized the filaments that had been polymerized in the presence of actin and Arp2/3 complex and did not generate new filaments. This method differs from the one used by Blanchoin et al. (*22*) and Amann et al. (*24*), in which phalloidin was present all throughout the polymerization process. In our hands, phalloidin greatly lowers the nucleation free energy, leading to the rapid assembly of G-actin into short filaments that anneal rapidly, thus profoundly interfering with the elongation and branching process (Samarin et al., unpublished data). The sample was incubated with phalloidin for 1 min, a period sufficient to stabilize filaments and short enough to minimize reannealing. The sample was then diluted 400-fold into F buffer containing 0.1% 1,4-diazabicyclo[2.2.2]octan (DABCO) as an oxygen scavenger, 10 mM DTT, and 0.1% methylcellulose. The solution (2 μL) was squashed between a microscope slide and a coverslip and processed for observation in a Reichert-Jung microscope using a Polyvar 100×/1.32 Oel

Iris objective and a Lhesa LH4046 analogue video camera. Branched and unbranched filaments (at least 200) were counted in several fields, recorded using a Panasonic AG-7355 video recorder. The percentages of unbranched and branched filaments were determined under each condition. The density of branching was defined as the number of branches formed per unit length of filaments, counting a total length of at least 2000 μm. The pictures were digitized and processed using a Scion Image software. This technique was used to estimate the kinetics of debranching. Samples were removed from the solution at different time intervals to determine the density of branches and the histogram of filament length distribution.

To discriminate between side branching and barbed end branching by Arp2/3 complex, a solution of preassembled filaments stabilized by Alexa-468 phalloidin was used as "green seeds". Spectrin-actin or gelsolin-actin initiated green seeds were tested in parallel. At time zero, 4 μM F-actin in green seeds was mixed with 5 μM G-actin, 0.2 μM ActA, and 30 nM Arp2/3 complex in polymerization buffer (G buffer containing 0.1 M KCl and 1 mM $MgCl_2$). After 3 min reaction, 5 μM rhodamine-phalloidin was added for 1 min and the sample was diluted 400-fold for observation in a Olympus AX70 fluorescence microscope, using a 100×/1.35 Oel Iris objective and a Lhesa LH 72LL camera, with appropriate filters for rhodamine and Alexa green fluorescence. Image processing was performed using the Metamorph software.

Reconstituted Actin-Based Motility of WT and Mutated Listeria and of ActA-Coated Microspheres with Pure Proteins. Bacteria were grown, stored frozen, washed, and placed in the reconstituted motility medium (*24*) containing the desired amounts of F-actin, Arp2/3, ADF, capping protein, VASP, and profilin. Polystyrene carboxylate-derivatized 1 μm diameter beads (Bangs laboratories, inc., Fishers, IN) were incubated at a concentration of 0.1% solids in X buffer (10 mM HEPES, pH 7.5, 0.1 M KCl, 1 mM $MgCl_2$, 0.1 mM $CaCl_2$, and 1 mM ATP) containing 0.7 μM full-length ActA, 0.1% BSA for 1 h on ice, sedimented, washed three times with X buffer and resuspended in X buffer at the original concentration. The beads were diluted 20-fold in the motility medium containing or not VASP. Movement of *Listeria monocytogenes* and of ActA-coated beads was monitored by phase contrast microscopy at room temperature, 10 min after preparation of the sample, in a Zeiss III RS microscope equipped with a Lhesa LHL4036 silicon-intensified camera. Movement was recorded in real time or time lapse using a Panasonic video recorder. Rates of movement were measured using a Hamamatsu image analyzer. At least 10 measurements were made on different bacteria for each sample. Average rates were derived from the distances moved over a period of 1 min. Standard deviations were calculated using the statistical tools of Kaleidagraph software.

RESULTS

Mutations in Regions of ActA Showing Sequence Similarity with VCA Inhibit Arp2/3-Induced Actin Polymerization. Mutations were generated in the region encoding ActA-N (see Experimental Procedures) to produce recombinant ActA-N variants. The same mutations were transferred onto the chromosome of *Listeria monocytogenes* by allelic exchange. Wild-type ActA-N and mutated ActA-N(Δ^{41}DEWEEE^{46}), ActA-N(W43A), ActA-N(^{146}KKRR^{149}-4A) fragments, the soluble full-length ActA protein, and the ActA(Δ 70−85) mutant were assayed for their ability to stimulate actin polymerization in the presence of Arp2/3 complex by monitoring the increase in pyrenyl-actin fluorescence (Figure 1). None of the ActA proteins affected the fluorescence of pyrenyl-G-actin. The polymerization curves in the presence of ActA-activated Arp2/3 displayed the same autocatalytic behavior as those obtained when Arp2/3 complex was activated by the C-terminal domain of N-WASp (*23*). As previously observed (*20*, *23*),

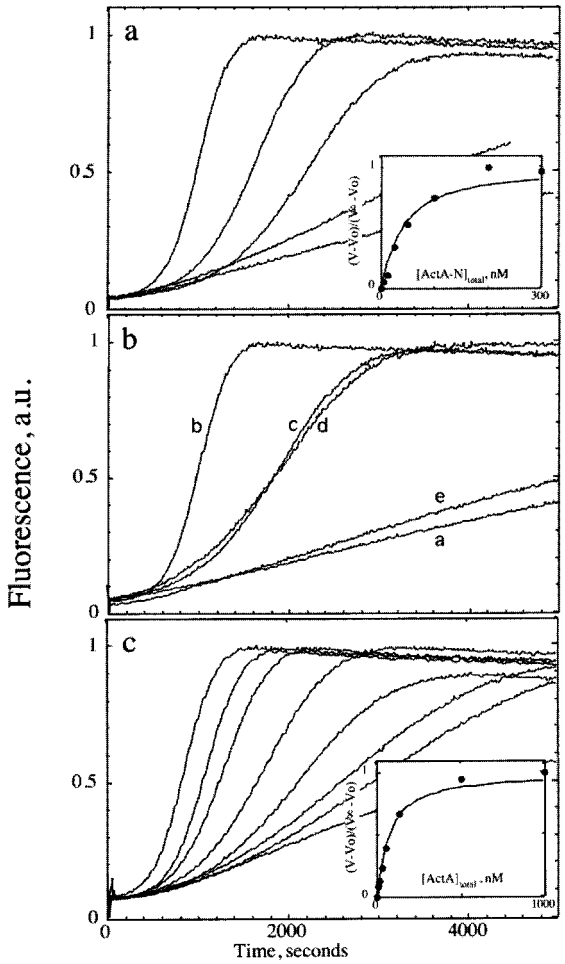

FIGURE 1: Activation of Arp2/3 complex by WT and mutated ActA protein stimulates actin polymerization. (a) Activation of Arp2/3 by wild-type N-ActA fragment. MgATP-G-actin (2 μM, 10% pyrenyl-labeled) was polymerized in the presence of 20 nM Arp2/3 and ActA-N at the following concentrations (bottom to top curves): 0, 6.25, 25, 50, and 200 nM. (Inset) Plot of the data according to eq 1 (see Experimental Procedures). The binding curve was calculated with $K = 30$ nM. (b) Mutated ActA-N activate Arp2/3 with a lower efficiency than ActA-N wild-type. Conditions as in panel a, with the following additions: a, none (actin + Arp2/3 alone); b, 0.2 μM ActA-N WT; c, 0.6 μM ActA-N(W43A); d, 0.6 μM ActA-N(Δ^{41}DEWEEE^{46}); e, 1.2 μM ActA-N(^{146}KKRR^{149}-4A). (c) Full-length ActA, but not ActA(Δ70−85), activates Arp2/3-induced polymerization of actin Conditions as in panel a, except the concentration of MgATP-G-actin is 2.5 μM, and ActA (top to bottom curves): 0, 5.4, 11, 27, 54, 135, 500, and 1000 nM. No activation was observed with ActA(Δ70−85) at concentrations up to 1.4 μM. (Inset) Plot of the data according to eq 1. The binding curve was calculated with $K = 60$ nM.

Table 1: Binding Parameters for the Interaction of ActA with G-Actin and Arp2/3 Complex[a]

species	Arp2/3 activation (K, μM)	G-actin binding (K', μM) inhibition of pointed end growth	G-actin binding (K', μM) depolymerization of gelsolin-capped filaments
ActA	0.06	4.5	6.5
ActA-N WT	0.03	1.5	2.2
ActA-N (W43A)	0.45	1.5	2.2
ActA-N(Δ^{41}DEWEEE^{46})	0.35	0.2	0.7
ActA-N (^{146}KKRR^{149}-4A)	>1	2.1	1.1

[a] Values of K and K', which reflect the interaction of ActA and different ActA variants with Arp2/3 and G-actin, respectively, were derived from the effects of ActA on the stimulation of actin polymerization by Arp2/3 (Figure 1), on the rate of filament growth and on the amount of depolymerized actin at steady state (Figure 4).

the time courses were not affected by the presence of BeF_3^-. Analysis of the data in terms of binding of ActA-N to an Arp2/3-containing active complex (see Experimental Procedures) yielded an equilibrium dissociation constant of 30 $\pm$ 10 nM for wild-type ActA-N (Table 1). The mutated ActA-N(Δ^{41}DEWEEE^{46}) and ActA-N(W43A) fragments activated Arp2/3 with K values of 0.35 and 0.45 μM, i.e., with a 1 order of magnitude lower affinity than WT ActA-N. The charged-to-alanine mutation of the ^{146}KKRR^{149} sequence has a more dramatic effect on the activation of Arp2/3 than the mutations or deletions of the acidic region. At concentrations up to 1 μM, the ActA-N(^{146}KKRR^{149}-4A) mutant did not show detectable activation of Arp2/3. The ActA-N(^{146}KKRR^{149}-4A) mutant abolished the activating effect of ActA-N wild-type, which suggests that the mutated ActA-N competes with the wild-type ActA-N for Arp2/3 binding, producing an inactive complex (data not shown).

Altogether, these results agree with the view (*28*) that the acidic region ^{41}DEWEEE^{46} and the region ^{146}KKRR^{149} of ActA, which show sequence similarity with the Arp2/3-binding "acidic" (A) and "cofilin homology" (C) regions of the C-terminal domain (VCA) of WASp and N-WASp, are involved in the activation of Arp2/3 by ActA.

Soluble full-length ActA activated Arp2/3 with a K value of 60 $\pm$ 10 nM (Figure 1c). At concentrations as high as 1 μM, ActA(Δ70−85), which does not bind G-actin (*29*), failed to activate Arp2/3. To determine whether ActA(Δ70−85) can still bind Arp2/3, polymerization assays were carried out in the presence of actin, Arp2/3 and ActA at fixed concentrations, and variable amounts of ActA(Δ70−85). If ActA(Δ70−85) competed with ActA for binding to Arp2/3, inhibition of the activation of polymerization would be observed as a result from the association of Arp2/3 in an inactive complex. Only 10 and 27% inhibition were observed when 1.9 and 4.8 μM ActA(Δ70−85) were, respectively, added to the reaction medium containing 0.1 μM ActA. In conclusion, the binding of ActA(Δ70−85) to Arp2/3 is extremely weak. The large deletion of the segment [70−85] of ActA may have caused a structural change sufficient to interfere with association of the protein with both Arp2/3 and G-actin.

ActA, ActA-N, and the VCA domain of N-WASp activated Arp2/3 complex identically when tested at the optimum concentrations (0.5 μM VCA, ActA, or N-ActA; data not shown). Overall, the present data, summarized in Table 1, suggest that the ability of ActA to bind both G-actin and Arp2/3 is involved in the activation of Arp2/3 complex to stimulate actin polymerization. No significant interaction of ActA or ActA-N with F-actin was found in sedimentation assays, in agreement with earlier data (*29*).

ActA has been shown to bind PIP2 (*29*, *37*). The effect of PIP2-containing liposomes on the activation of Arp2/3 by ActA was assayed. PIP2 inhibited the activation process up to 100% in a dose-dependent fashion, with a K_d of 7−10 μM in three independent experiments (data not shown). It is likely that, as proposed (*29*), PIP2 regulates the interaction of ActA with Arp2/3 complex by preventing the formation of the activated Arp2/3 complex. PIP2 could destabilize the interaction of either Arp2/3 or G-actin with ActA.

Immunofluorescence Study of the Listeria Mutants in Infected Cells. The ability of the ActA mutants (Δ^{41}DEWEEE^{46}, W43A, and ^{146}KKRR^{149}-4A) to induce actin polymerization in vivo was analyzed in infected HeLa cells (Figure 2a). All three mutants displayed a positive ActA staining (100% of the bacteria). Almost all (98%) wild-type bacteria induced actin polymerization, and 80% of them displayed actin tails of average length 8.3 $\pm$ 1.5 μm (N = 17). The isogenic strains expressing ActA-N(Δ^{41}DEWEEE^{46}) and ActA-N(W43A) induced actin polymerization (95%) and 30% of the bacteria displayed short actin tails of average length 3.1 $\pm$ 1.6 μm (N = 15). Hence, the 10-fold decrease in affinity of the ActA mutants for Arp2/3 complex is not sufficient to abolish motility. In contrast, bacteria expressing ActA(^{146}KKRR^{149}-4A) did not induce actin polymerization and failed to move, in agreement with the results of in vitro polymerization assays. Arp2/3 complex was present (97−98%) around the bacteria and in the actin tails for wild-type and mutants expressing ActA(Δ^{12}DEWEEE^{17}) and ActA-(W43A) (not shown), but was not detected around bacteria expressing ActA(^{146}KKRR^{149}-4A). These results are in agreement with the present biochemical data and with recent works (*28*, *40*).

Motility of the Listeria Mutants in the Reconstituted Motility Medium. So far only the movement of *L. monocytogenes* strain L028 actA::Tn917lac (pactA3) overexpressing ActA (*41*) has been monitored in a motility medium reconstituted from pure proteins (*25*). The wild-type *Listeria* L028 strain, which expresses ActA (less efficiently) from its chromosome, failed to move in vitro in *Xenopus* egg or human platelet extracts. Wild-type *Listeria* L028 in contrast moved actively at 1−1.5 μm/min in the minimum motility medium (Figure 2b). The strains expressing mutated ActA(W43A) or ActA(Δ^{41}DEWEEE^{46}) moved much more slowly (<0.1 μm/min) and showed short actin tails. The strains expressing ActA (^{146}KKRR^{149}-4A) and ActA(ΔN-term) failed to induce actin assembly at their surface and did not move. In an attempt to improve the motility of the *Listeria* harboring mutated ActA-W43A and ActA-Δ^{41}DEWEEE^{46}, the composition of the motility medium was modified by increasing the concentration of Arp2/3 complex up to 0.7 μM, hoping to compensate for the low affinity of Arp2/3 for the mutated ActA. The rate of movement of the mutant *Listeria* was not appreciably affected. However, in a control assay carried out at this high concentration of Arp2/3, wild-type *Listeria* moved more slowly. The results of in vitro motility assays, summarized in Table 2, are in agreement with the immunofluorescence observations of the same

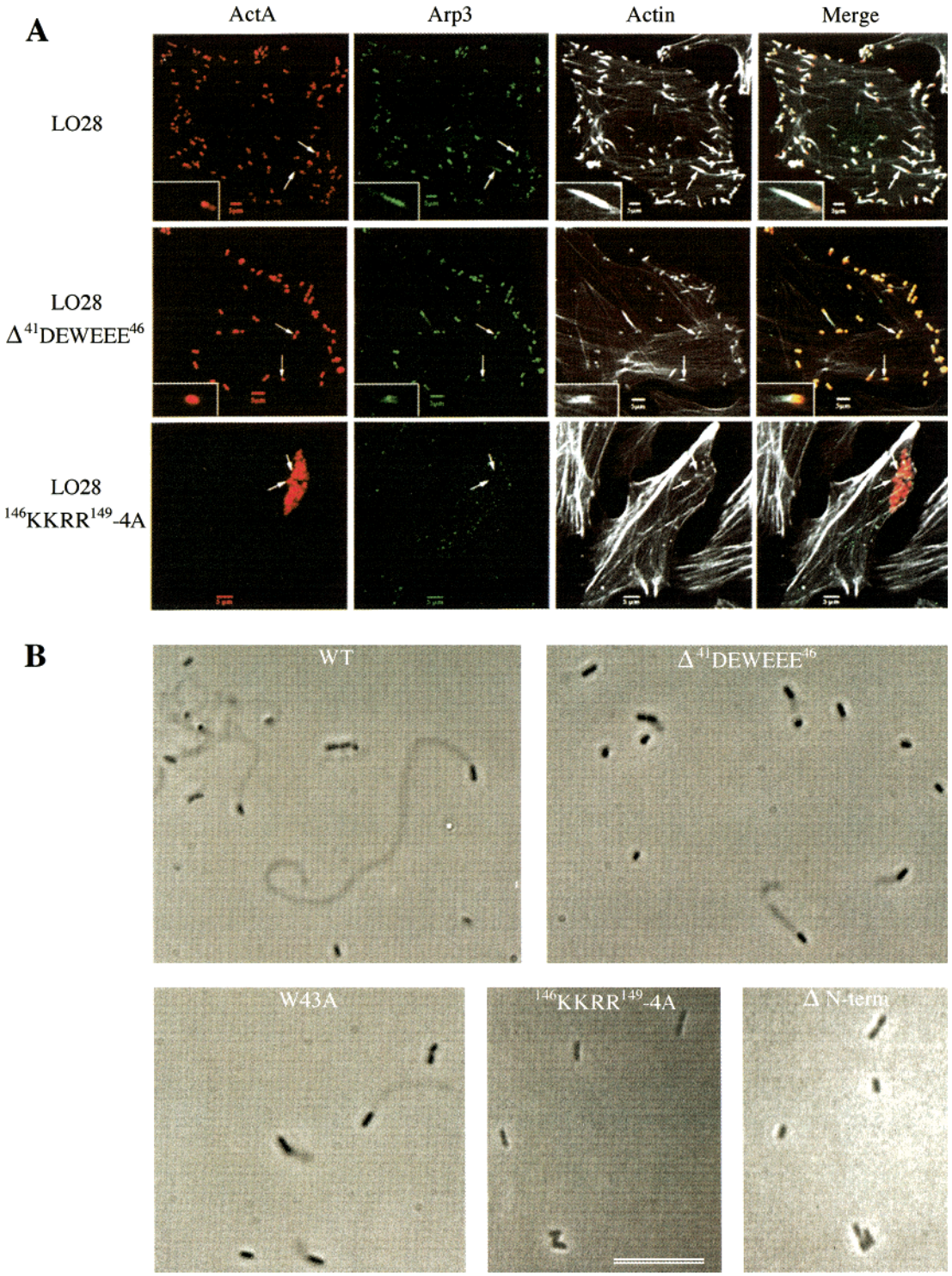

FIGURE 2: Motility of Listeria L028 wild-type and mutants. (a) Motility in infected cells. Bacteria are labeled with anti-ActA A16 antibody (red). Arp2/3 is detected with an anti-Arp3 antibody (green). Actin is revealed with FITC-phalloidin. Note that in contrast with wild-type L028, the ^{146}KKRR^{149}-4A mutant does not recruit Arp2/3 and does not induce actin polymerization. The L028 Δ^{41}DEWEEE^{46} recruits Arp2/3 and induces actin assembly, but the proportion of bacteria showing tails is lower than for wild-type L028 and actin tails are shorter than those displayed by wild-type L028. (b) Motility in the reconstituted motility medium. Typical phase contrast images of *Listeria* BOF 343 wild-type and mutants as indicated in the reconstituted motility medium. The ActA wild-type, ActA(Δ^{41}DEWEEE^{46}) and ActA(W43A) strains are motile, while the strains ActA(^{146}KKRR^{149}-4A) and ActA(ΔN-term) are nonmotile. Bar = 10 μm.

strains in infected cells, suggesting that the composition of the motility medium is close to physiological.

ActA Activates Filament Barbed End Branching by Arp2/3. Fluorescence microscopy observation of filaments polymerized in the presence of Arp2/3 and ActA or ActA-N wild-type showed a mixture of branched and nonbranched filaments immediately following attainment of the steady state of polymerization (Figure 3). Identical densities of branching were measured with full-length ActA and WT ActA-N. The lengths of mother and daughter branches were measured on the recorded video-microscopy images of rhodamine-phalloidin stained filaments, prepared as described

Table 2: Rate of Movement and Mean Length of Comet Tails of Different *Listeria* Strains in the Motility Medium[a]

	WT	W43A	Δ^{41}DEWEEE^{46}	^{146}KKRR^{149}-4A
rate of movement, μm/min (number of measurements)	1.42 ± 0.36 (13)	<0.1 (15)	<0.1 (10)	no polymerization of actin
mean length, μm (number of measurements)	26.12 ± 10.23 (12)	5.66 ± 2.53 (15)	7.16 ± 3.48 (10)	

[a] Only the ActA wild-type, ActA(W43A), and ActA(Δ^{41}DEWEEE^{46}) strains were motile in the motility medium. The ActA(^{146}KKRR^{149}-4A) mutated *Listeria* showed no actin polymerization at their surface. Measurements of comet tail length were taken 1 h after the establishment of steady-state movement.

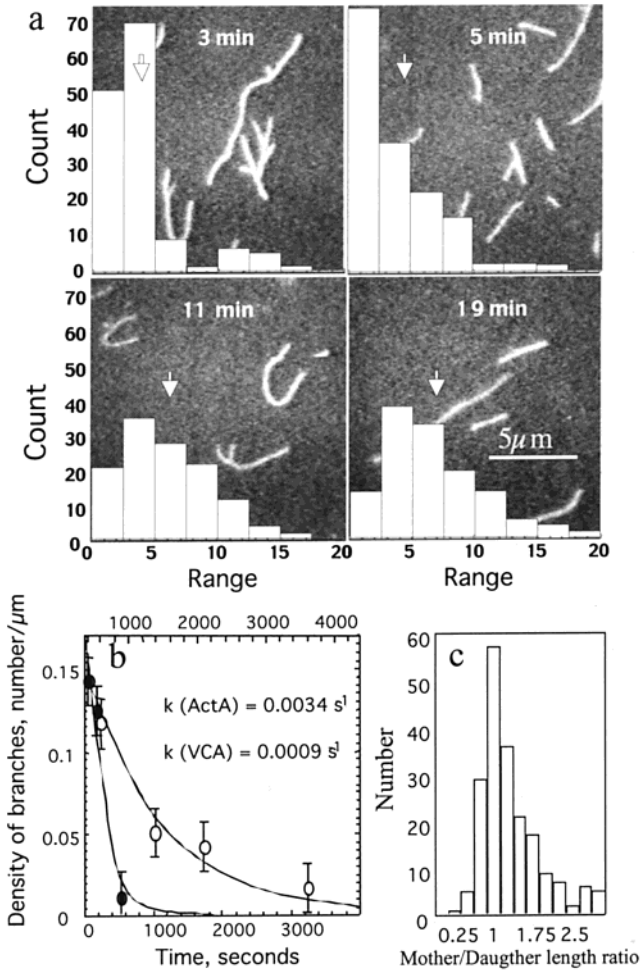

FIGURE 3: ActA-activated Arp2/3 complex promotes barbed end branching of filaments followed by debranching and redistribution in length. (a) Fluorescence microscopy evidence for filament branching and debranching. Mg-ATP-actin (5 μM) was polymerized in the presence of 30 nM Arp2/3 and 0.6 μM ActA. At the indicated times, filaments were observed by rhodamine phalloidin staining. Typical fields are shown. Bar = 5 μm. Histograms of length distribution were derived from the recorded data at the same time points. (b) Time dependence of the density of branches upon polymerization of MgATP-actin (5 μM) with 30 nM Arp2/3 and either 1 μM VCA (open circles) or 0.6 μM ActA (closed circles). (c) Histogram of the mother/daughter length ratio of filaments assembled for 3 min in the presence of G-actin, ActA, and Arp2/3 complex (conditions as in panel a).

in the Experimental Procedures (i.e., phalloidin was added to polymerized filaments, not to G-actin). A histogram of the distribution of the ratio of the lengths of mother and daughter branches (Figure 3) shows that a majority of mother and daughter branches were equal in length, as previously observed in EM (*23*). The proportion of branched filaments decreased exponentially with time. The debranching process was about 3-fold faster with ActA ($k = 0.003 \pm 0.001$ s^{-1}) than with VCA ($k = 0.0009 \pm 0.0002$ s^{-1}). Because of the rapid debranching observed with ActA, in several experiments branched filaments were barely detectable after 10 min. These results confirm, in agreement with our previous results with Arp2/3 activated by the VCA of N-WASp (*23*), that debranching occurs after the formation of branched filaments. Debranching has also been observed with the VCA of WASp (*23*). It is known that inorganic phosphate (Pi) is released at a rate of 0.006 s^{-1} ($t_{1/2} = 100$ s) from Mg-ADP-Pi-F-actin (*42*), appreciably faster than the debranching rate. In our hands, addition of 20 mM sodium phosphate (which is known to stabilize filaments) or 1 mM BeF_3^- to the polymerizing solution and to the dilution buffer used for microscopy (keeping the ionic strength constant) did not detectably prevent nor slow debranching. Blanchoin et al. (*43*) observed a partial and weak slow of the debranching process by BeF_3^-. Histograms of length distribution of filaments observed at different times of the polymerization process show that debranching is accompanied by the redistribution in length of filaments (Figure 3, top panel) to a lower number concentration of longer filaments. The redistribution process was verified using a seeded polymerization assay (data not shown) which confirmed that the number of filaments decreased by 3-fold in 1 h following attainment of steady state.

To determine whether ActA-activated Arp2/3 complex promotes the formation of branched filaments by binding to the sides or to the ends of filaments during polymerization, the following experiment was carried out (Figure 4). Solutions of F-actin nucleated by spectrin-actin (1.5 μM actin and 1 nM spectrin-actin seeds) or by gelsolin (2 μM actin and 1 nM gelsolin) containing the same number of filaments with either free barbed ends (spectrin-actin-nucleated) or gelsolin-capped barbed ends, and the same mass amount of F-actin (1.4 μM, because the critical concentrations are 0.1 and 0.6 μM at the barbed and pointed end, respectively) were prepared. An aliquot of these solutions (final concentrations: 20 pM filament ends, 28 nM F-actin subunits, corresponding to 4 μm long filaments on average) was added at time zero together with salt to a solution of 2.2 μM Mg-ATP-G-actin, 10.6 nM Arp2/3 complex, and 0.6 μM ActA. The time courses of actin assembly in the samples supplemented or not with F-actin were recorded simultaneously. The activation period was shortened by addition of filaments at time zero only if the filaments had free barbed ends. The gelsolin-capped filaments, which contained the same amount of F-actin available for side-binding of Arp2/3 as the spectrin-actin nucleated filaments, failed to shorten the activation period. Moreover, addition of 20 pM spectrin-actin seeds (i.e., barbed end nuclei), with no F-actin, shortened the

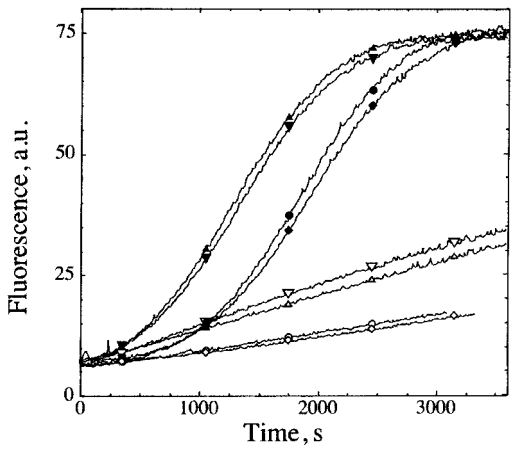

FIGURE 4: ActA-activated Arp2/3 complex branches filaments from the barbed ends. Closed symbols: Mg-ATP-G-actin (2.2 μM, 10% pyrenyl-labeled) was polymerized in the presence of 10.6 μM Arp2/3 complex and 0.6 μM ActA, in the absence (circles) or in the presence of spectrin-actin nucleated filaments (28 nM F-actin, 20 pM ends, pointing up triangles) or of gelsolin-capped filaments (28 nM F-actin, 20 pM ends, diamonds), or in the presence of 20 pM spectrin-actin seeds (no filaments, pointing down triangles). Open symbols: corresponding control curves in the absence of Arp2/3 complex.

activation period to the same extent as the 20 pM spectrin-actin nucleated, 4 μm long, filaments. These results demonstrate that ActA-activated Arp2/3 complex, like WA-activated Arp2/3 complex, interacts with the barbed ends rather than with the sides of filaments to initiate branching. This result is in good agreement with the frequent equal lengths of mother and daughter branches (Figure 3).

Note that the use of gelsolin, which has a very high affinity ($K_d \ll 0.1$ nM) for barbed ends, is crucial in this experiment. In a similar experiment using filaments capped by *Acanthamoeba* capping protein as seeds, the opposite result was obtained (*24*). However, because *Acanthamoeba* capping protein binds barbed ends with a K_d as high as 5 nM (*43*), an appreciable amount of non capped filaments, as judged from the control curve (no Arp2/3) in which barbed end growth from profilin-actin was detected, accompanied the addition of a large number of short barbed end-capped filaments. This experiment therefore does not conclusively distinguish between side branching and barbed end branching because the barbed ends contaminating the capped filaments may have led to activation of Arp2/3 complex. This problem is avoided here by using gelsolin, a high affinity capping protein.

The above experiment was complemented with video-microscopy observations of branched filaments in which Alexa 468-phalloidin stabilized filaments were added as seeds to a solution of G-actin, ActA and Arp2/3 complex (see Experimental Procedures). Newly formed filaments were stained with rhodamine-phalloidin. A mixed population of green and red branched filaments was analyzed. A statistic evaluation of the different types of branches was performed (Figure 5). Ninety percent of the branches consisted of red mother and red daughter filaments that either had assembled spontaneously or had elongated from the green seeds. Red daughter filaments attached to the sides of green filaments represented 2% of the branches and were seen as frequently as green daughter filaments attached to the sides of red or green mother filaments. These rare apparent side branching events are unlikely to represent a relevant function of Arp2/3 complex. Similar rare images of end-to-side attachment of filaments were also observed upon mixing Alexa-green phalloidin-stabilized filaments and rhodamine-phalloidin-stabilized filaments in the absence of Arp2/3 complex. Data identical to those displayed in Figure 5 (with reversed colors) were obtained using seeds made from rhodamine-labeled F-actin (non-phalloidin-stabilized) and staining the newly assembled filaments with Alexa 468-phalloidin. Hence, barbed end branching occurs from either phalloidin-stabilized or nonstabilized filaments. In conclusion, all our results are consistent with barbed end branching by Arp2/3 complex and show no compelling evidence for side branching.

The above microscopy data also provide evidence for reannealing of filaments. Only filaments containing two "green seed" segments, i.e., showing a minimal green-red-green sequence must have been unambiguously formed by reannealing, and represent 2 among 16 identically probable reannealing events. The other 14 events are not visualized in the two-stain assay and represent the "hidden part of the iceberg". A proportion of 3% of the filaments showed a green-red-green pattern, indicating that 24% of the filaments must have reannealed even when phalloidin is added at late times of the polymerization process.

The Complex of ActA with G-Actin Associates Productively to Barbed Ends, Like Profilin-Actin or WA-Actin. To address whether ActA activates Arp2/3 complex like VCA, by forming a ternary complex with both G-actin and Arp2/3, the binding of ActA to G-actin was evaluated in kinetic and steady-state polymerization measurements.

The growth of filaments from G-actin subunits was inhibited at the pointed end, not at the barbed end (Figure 6a) by ActA, ActA-N, ActA-N(Δ^{41}DEWEEE^{46}), ActA-N(W43A), and ActA-N(^{146}KKRR^{149}-4A). In contrast, ActA(Δ70−85) did not inhibit pointed end growth at concentrations up to 20 μM (data not shown). The inhibition of pointed end growth was analyzed in terms of ActA binding to G-actin in a 1:1 complex that does not participate in filament elongation at the pointed end (see Experimental Procedures). Using a similar assay, Zalevsky et al. (*31*) concluded that ActA bound two G-actin monomers. As will be clarified in the Discussion, the difference with the present conclusion is not in the data, but in the analysis of the data. The values of the equilibrium dissociation complex for all ActA variants binding to G-actin are summarized in Table 1 and fall in the range of 1.5−4.5 μM, except for the ActA-N(Δ^{41}DEWEEE^{46}) mutant which has a 10-fold higher affinity ($K' = 0.2$ μM) for G-actin.

Accordingly, when added to F-actin, all ActA variants [but not ActA(Δ70−85)] caused depolymerization of gelsolin-capped filaments and shifted the pointed end critical concentration plots (Figure 6, panels b and c) consistent with a G-actin sequestering activity. Values of the equilibrium dissociation constant for the ActA-G-actin complexes (K') of 0.7−6 μM were derived from the data (Table 1) and are in satisfactory agreement with the values of K' derived from the inhibition of pointed end growth. In conclusion, all ActA mutants (except ActAΔ70−85) show affinities for G-actin similar to or higher than wild-type ActA, which contrasts with the large difference in activity of wild-type and mutated ActA-N in the Arp2/3-stimulated polymerization assay.

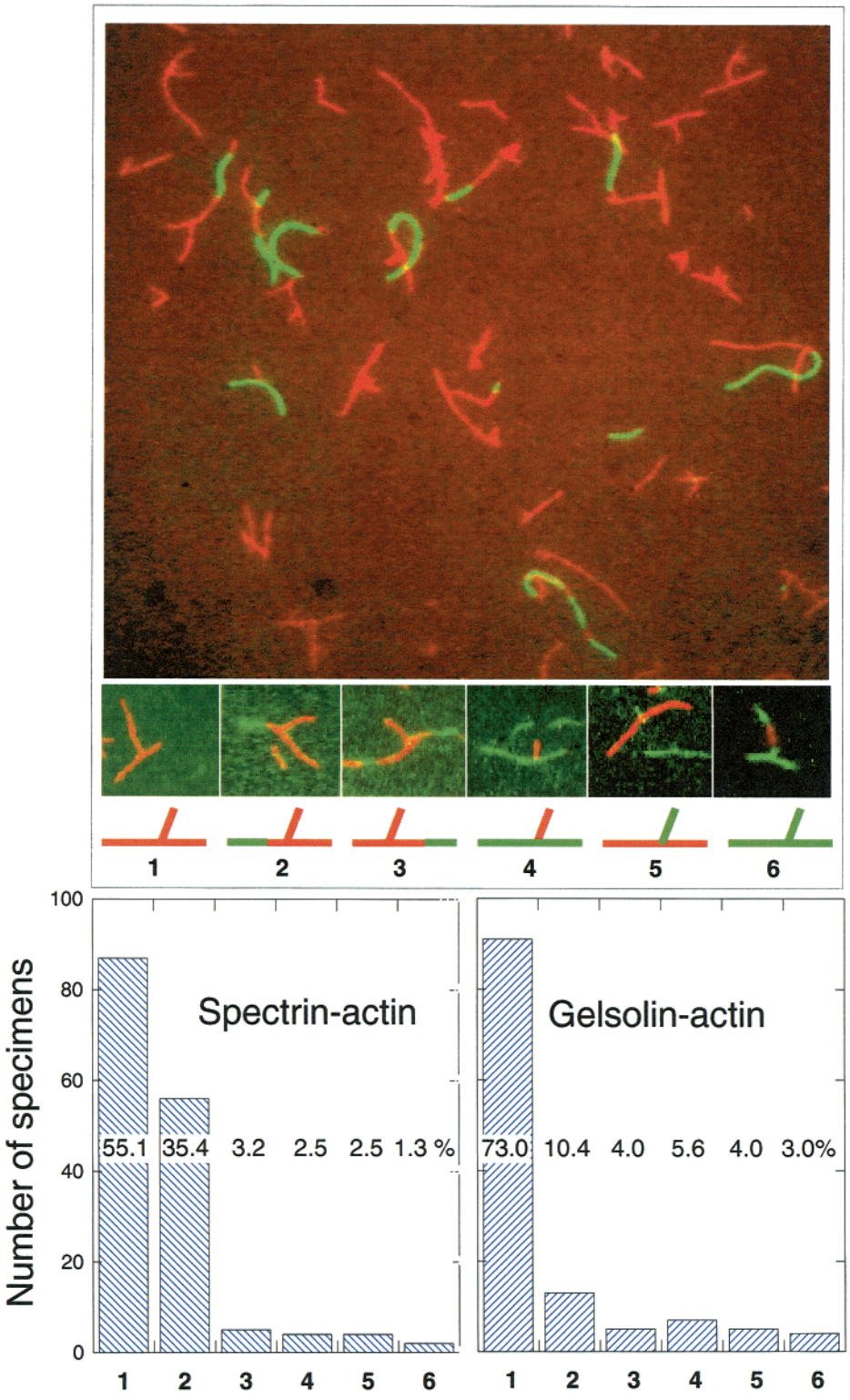

FIGURE 5: Fluorescence micrographs of filaments assembled in the presence of Alexa 468-phalloidin-stabilized filaments ("green seeds") and Arp2/3 complex. Alexa 468 phalloidin-F-actin (4 μM) was mixed at time zero with 5 μM G-actin, 0.2 μM full-length ActA, and 30 nM Arp2/3 complex. Rhodamine phalloidin was added after 3 min. Dilution in fluorescence buffer and observation were carried out at time 4 min. (Top panel) Typical field showing a mixed population of green and red filaments. Note the occurrence of reannealing illustrated by a green-red-green filament at the bottom of the image. The observed images of branches fall into six classes (numbered 1−6), illustrated and drawn schematically. (Bottom panel) Statistical analysis of the distribution of the different types of branched filaments into the six classes defined above, when the green seeds were initiated from spectrin-actin or gelsolin-actin as indicated.

When barbed ends were free, none of the ActA variants caused F-actin disassembly (Figure 6c). In conclusion, ActA, like the VCA of N-WASp (*16*), does not bind actin like a pure G-actin-sequestering protein, but like profilin and like VCA. The ActA-G-actin complex productively associates with barbed ends.

PIP2, at concentrations up to 50 μM, did not affect the inhibition of pointed end growth by ActA (data not shown).

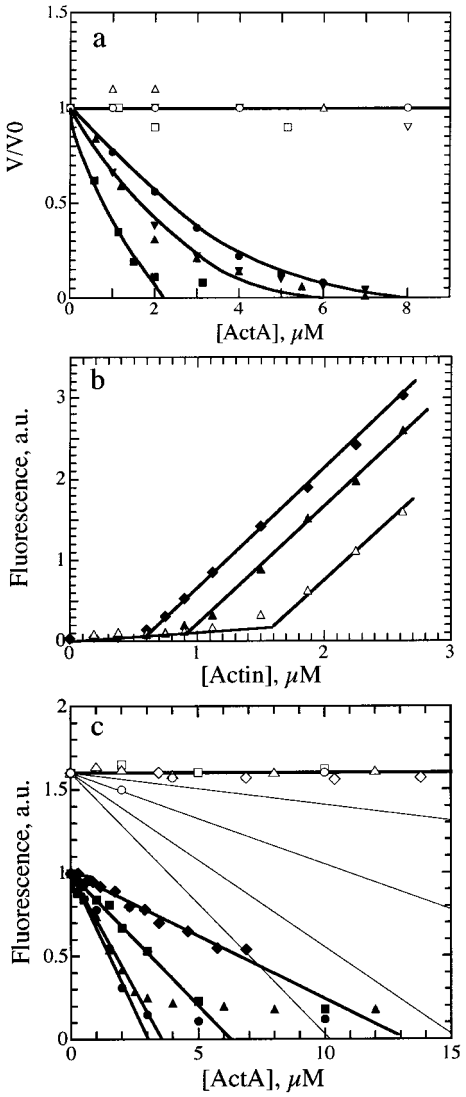

FIGURE 6: One-to-one complex of ActA with G-actin associates productively with filament barbed ends exclusively. (a) ActA inhibits filament growth from the pointed end, not from the barbed ends. Pointed end growth (closed symbols) was measured in the presence of 2 μM G-actin and the different N-ActA fragments: triangles, WT N-ActA; up-side-down triangles, N-ActA W43A; squares, N-ActAΔ^{41}DEWEE^{46}; circles, N-ActA^{146}KKRR^{149}-4A. Curves are calculated using eq 2 with the best fit values of K' for binding of ActA to G-actin given in Table 1. Data for full-length ActA (Table 1) were obtained at a different actin concentration (2.5 μM) and cannot be represented on the same graph. The rate of barbed end growth (open symbols) is measured similarly using spectrin-actin seeds. (b) ActA shifts the critical concentration plots at the pointed end by sequestering G-actin. Critical concentration plots of gelsolin-capped F-actin were carried out in the absence (diamonds) or presence of N-ActAW43A at 1.88 μM (closed triangles) or 5 μM (open triangles). Values of K' of 2.3 μM and 2.1 μM were derived from the data. Similar data were obtained with ActA and ActA-N, as further shown in panel c. (c) Compared G-actin binding activities of the different ActA variants. The G-actin sequestering activity of full-length ActA (diamonds), N-ActA WT (squares), ^{146}KKRR^{149}-4A (triangles), Δ^{41}DEWEEE^{46}(circles), were compared by measuring the decrease in F-actin (1.5 μM total actin) at steady state in the presence of the indicated amounts of ActA. Closed symbols, gelsolin-capped filaments (gelsolin:actin =1:300); open symbols, non capped F-actin. Thin lines represent calculated curves expected if the ActA-G-actin complex did not participate in assembly at the barbed ends, and using the values of K derived from the 4 experimental linear curves at the pointed ends. The data points do not fall on those lines, showing that no sequestering activity is observed when barbed ends are not capped.

Therefore the inhibitory effect of PIP2 on the ActA-Arp2/3-stimulated actin polymerization is likely due to an inhibition of the ActA-Arp2/3 interaction, not of the G-actin-ActA interaction, in agreement with previous findings (*29*).

VASP Does Not Affect Barbed End Branching by ActA-Activated Arp2/3. ActA possesses a central domain containing four proline-rich repeats that bind the N-terminal EVH1 domain of VASP, a protein which enhances actin-based motility of *Listeria* (*30*, *44*, *38*, *25*). The EVH1 domain and the C-terminal EVH2 domain of VASP, which binds F-actin weakly, are both required for the effect of VASP, which is independent of profilin (*38*). A crucial issue is whether the mechanical effect of VASP in motility is associated with some regulation of the filament branching activity of ActA-Arp2/3, or the growth of barbed ends at the surface of *Listeria*. Before setting up biochemical assays to address this issue, it was important to know whether VASP affects the propulsion of ActA-coated beads, as it does for bacteria, in the chemically controlable reconstituted motility medium. Polystyrene beads (1 μm in diameter) were incubated with full-length soluble ActA at different concentrations as described (*45*) and placed in the minimum motility medium containing VASP at known concentrations in the range 0 to 1 μM.

In the absence of VASP, ActA-coated beads initiated the formation of an actin cloud, escaped the cloud in a step of break of symmetry (*46*), but rapidly stopped moving afterward (Figure 7a, top panel). In the presence of VASP at 0.5 μM and above, the beads moved steadily for hours at 2 μm/min with normal comet tails (Figure 7a, bottom panel). At VASP concentrations between 0 and 0.5 μM, faint comet tails were formed and disassembled within 15−30 min, with arrest of movement. The beads did not resume movement thereafter. Control assays carried out in parallel with *Listeria* overexpressing ActA (strain Lut12) reproduced the effect of VASP published earlier (*25*), i.e., in the absence of VASP the bacteria displayed normal tails and very slow sustained movement, and moved 10-fold faster in the presence of VASP. Wild-type *Listeria*, which express a low density of ActA at their surface, did not move in the absence of VASP. In conclusion, VASP improves the motility of both ActA-coated beads and bacteria. The difference between the beads and the bacteria lies in the arrest of movement of beads in the absence of VASP after a short while.

The effect of VASP on actin-based movement could be mediated by its modulation of the filament branching activity of ActA-Arp2/3 complex or the rate of debranching. Alternatively, VASP interaction with ActA could affect the growth of actin filaments in the context of the motility assay, i.e., in the presence of capping proteins; for instance, VASP could inhibit the binding of capping proteins to barbed ends soon after the formation of a branch, thus favoring growth and improving speed. VASP might also interact with Arp2 and/or Arp3 in the Arp2/3 complex, via its EVH2 domain. These possibilities have been addressed in the following experiments.

The putative interaction of VASP with Arp2/3 complex was tested in a pull-down assay. Immobilized His-tagged VASP was incubated with Arp2/3 complex. The binding of Arp2/3 to VASP was measured by western blotting. This assay failed to detect a significant binding of VASP to Arp2/3

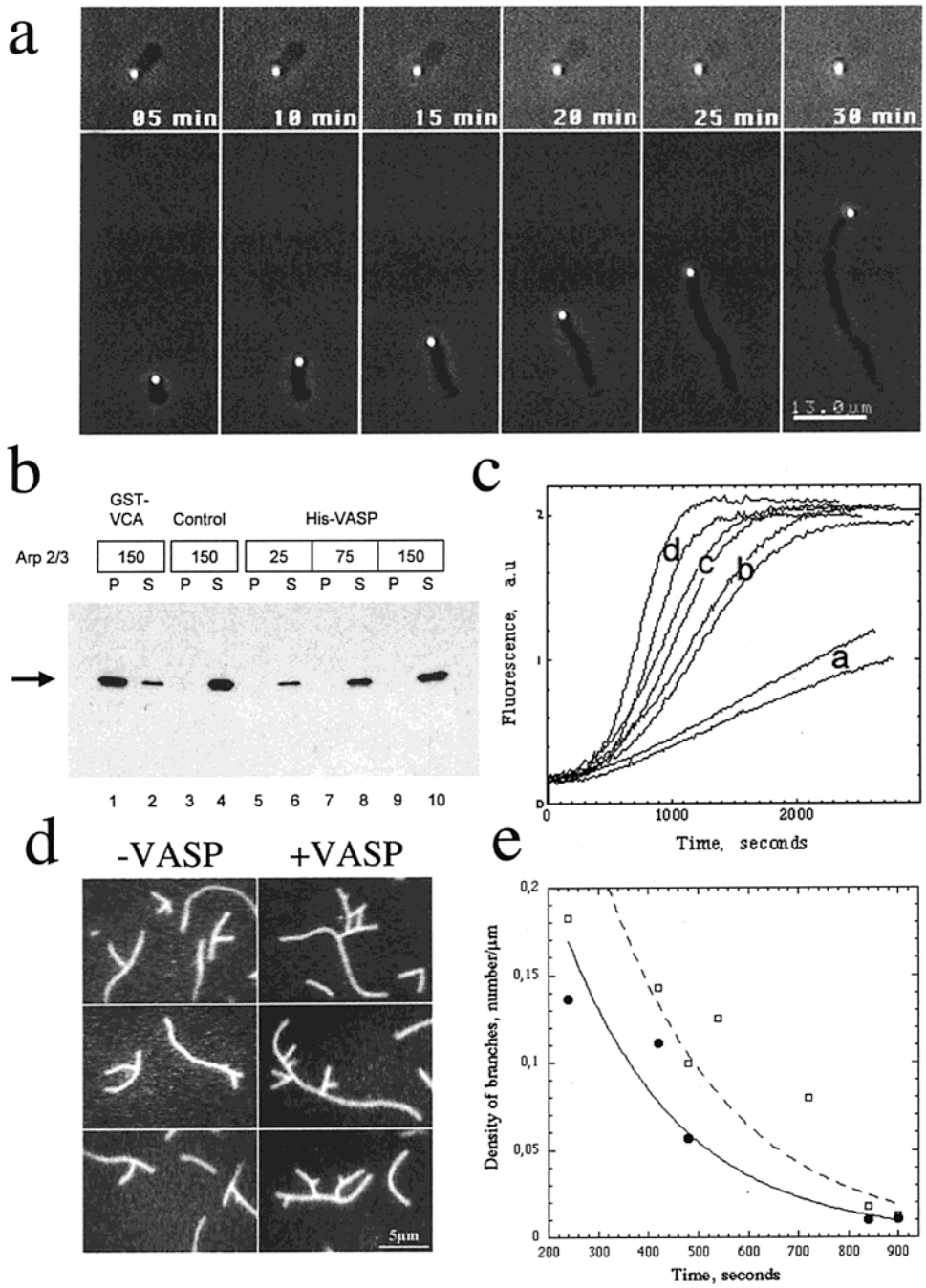

FIGURE 7: VASP improves the motility of ActA-coated beads but does not affect filament branching by ActA-activated Arp2/3. (a) VASP is required for sustained motility of ActA-coated beads. Time lapse recorded movement of 1 μm diameter ActA-coated beads in the reconstituted motility medium without VASP (top) and with 0.5 μM VASP (bottom). (b) VASP does not interact with Arp2/3 complex. One nanomole of His-tagged VASP immobilized on 20 μL of Ni agarose beads were added to 25, 75, or 150 pmol of Arp2/3 complex (lanes 5−10). One nanomole of GST-VCA immobilized on 20 μL glutathione sepharose beads were added to 150 pmol of Arp2/3 complex as a negative control (lanes 3 and 4). The presence of Arp2/3 in the supernatant (S) and washed beads (P) was detected using a polyclonal anti-Arp3 antibody. (c) VASP has no effect on the stimulation of actin polymerization by ActA-activated Arp2/3 complex. MgATP-G-actin (2.5 μM, 10% pyrenyl-labeled) was polymerized in the presence of 15 nM Arp2/3 and full-length ActA at the following concentrations. a, 0; b, 26 nM; c, 52 nM; d, 260 nM. Thin and thick lines represent the recorded time courses of pyrenyl-actin fluorescence in the absence or presence of 0.2 μM VASP, respectively. (d) Typical images of tetramethylrhodamine-phalloidin-labeled branched filaments assembled in the presence of ActA, Arp2/3 and in the absence or presence of VASP as indicated. MgATP-G-actin (5 μM) was polymerized in the presence of 0.2 μM ActA, 30 nM Arp2/3, and without 0.15 μM VASP for 7 min before phalloidin addition and observation in fluorescence microscopy. Bar = 5 μm. (e) VASP does not greatly affect the rate of filament debranching. The density of branches was measured at different times following attainment of the steady state. Conditions are as in panel d. Data points from two independent sets of experiments (each set without VASP) are combined.

complex (Figure 7b). A parallel control assay showed that Arp2/3 bound tightly to VCA-loaded beads.

The effect of VASP on the activation of Arp2/3 complex by ActA in solution was addressed in polymerization assays (Figure 7c). At concentrations up to 0.5 μM, VASP did not detectably affect the stimulation of actin assembly by Arp2/3 complex, in a range of ActA concentrations (0−0.2 μM). Using a seeded polymerization assay, the same number of

filaments were found when actin was polymerized with ActA and Arp2/3 complex, in the presence or absence of VASP. The steady-state rate of ATP hydrolysis measured when 5 μM actin was polymerized with 0.2 μM ActA and 30 nM Arp2/3 complex was 3 nM/s (15-fold higher than in the absence of Arp2/3 complex) and was unaffected by VASP, testifying that the same number of filaments were formed (data not shown). At concentrations higher than 0.5 μM, VASP in itself displayed a weak actin-nucleating effect, independently of Arp2/3, due to the interaction of its C-terminal EVH2 domain with F-actin (*38*). This nucleating effect might provide free barbed ends available for branching by Arp2/3; however, no synergy between VASP and Arp2/3 was observed.

The potential interplay between capping proteins and VASP was addressed by monitoring actin polymerization in the presence of ActA, Arp2/3 complex, and capping proteins, in the presence or absence of VASP. Again superimposable polymerization curves were obtained, demonstrating that VASP does not interfere with barbed end capping (data not shown). A confirmatory experiment was carried out as follows. We have shown (*23*) that VCA-activated Arp2/3 complex creates new barbed ends in a medium containing barbed end-capped filaments, which results in the lowering of the steady-state ATP-G-actin concentration. Addition of increasing amounts of ActA-activated Arp2/3 complex to a solution of gelsolin capped filaments also caused a decrease in the steady-state concentration of ATP-G-actin, in the exact same fashion with and without VASP. These steady-state measurements confirm that VASP does not affect the interplay between barbed end branching and capping.

In agreement with the above polymerization assays, when filaments assembled in the presence of ActA, Arp2/3, and VASP and stabilized by rhodamine-phalloidin were observed in the optical microscope, at the same polymerization time the extent of filament branching was only slightly higher than when they were assembled in the absence of VASP, and multiply branched filaments were frequently observed. The rate of debranching was not appreciably modified by VASP (Figure 7e).

DISCUSSION

We have shown that the *Listeria* protein ActA activates Arp2/3 complex to multiply filaments at the surface of *Listeria* by barbed end branching, using the same molecular mechanism as proteins of the WASp family, the natural activators of Arp2/3 in eukaryotic cells. Activation of Arp2/3 complex implies that ActA interacts with both G-actin and Arp2/3 in a ternary complex, mimicking the interaction of the C-terminal VCA domain of WASp with G-actin and Arp2/3. The ActA-N fragment and the full-length ActA protein equally activate Arp2/3. Therefore, the active N-terminal domain of ActA is exposed in the full-length protein, in contrast with WASp proteins.

Reported discrepancies (*28*, *31*) concerning the role of different regions of ActA in Arp2/3 complex activation have been resolved here by quantitative assays. ActA binds G-actin with an affinity in the 10^6 M^{-1} range and activates Arp2/3 with an affinity in the 10^7-10^8 M^{-1} range. Previous studies (*29*, *30*) strongly suggest that the sequences ^{71}DIKELEKSNK^{80} and ^{93}LKEKAEK^{99} in the central part of

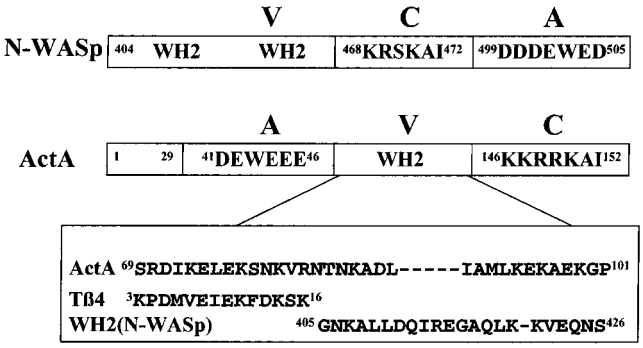

FIGURE 8: Domain organization of the N-terminal domain of ActA and alignment with the C-terminal domain of N−WASp. The "acidic" (A) DEWE sequence, the "cofilin homology" (C) sequence, and the verprolin homology (V) region are featured in ActA and VCA. The sequence similarities to Tβ4 and to the verprolin homology region of N-WASp are outlined in the box.

ActA-N, similar to the actin binding motif found in β-thymosins, are part of the actin binding site in ActA. In contrast, it was proposed (*31*) that the sequence [121−138] was a verprolin homology region. This sequence alignment required the introduction of several gaps. Moreover, a [120−612] ActA fragment did not display the functional properties of full-length ActA, suggesting that its binding to actin resulted from a nonphysiological folding of the protein. The conserved ^{41}DEWEEE^{46} and ^{146}KKRRA^{150} sequences, known to play a role in ActA function (*30*, *28*, *41*), are shown here to be involved in Arp2/3 binding, not in G-actin binding. Mutations in the acidic ^{41}DEWEEE^{46} sequence in ActA cause a 10-fold decrease in affinity for Arp2/3 complex. This result accounts well for the slower motility of the mutated strains in living cells and in the reconstituted motility medium. In contrast, the charged-to-alanine mutation of the ^{146}KKRR^{149} sequence causes a severe impairment of ActA function. We find, at variance with Skoble et al. (*28*), that the binding of this mutated ActA to G-actin is not affected but its interaction with Arp2/3 complex leads to the formation of a dead-end Arp2/3-ActA-G-actin complex (data not shown). The attribution of the Arp2/3 binding regions on ActA differs from Zalevsky et al. (*31*), who placed a putative acidic consensus sequence (^{166}DKPTK^{170}) adjacent to the C-terminus of the cofilin homology region, so as to keep the same sequence arrangement (verprolin homology, cofilin homology, acidic region) in ActA as in the VCA domain of WASp and N-WASp. In agreement with Skoble et al. (*28*), our data indicate that in ActA the actin binding region is inserted between the two regions (acidic and basic) which bind Arp2/3, leading to a AVC sequence arrangement. Nevertheless, the 3D structure of ActA and VCA interfaces with actin and Arp2/3 might be very similar. The compared domain arrangements of VCA and ActA, showing the actin-binding sequences similar to β-thymosin and verprolin homology region of N-WASp, are displayed in Figure 8. The fact that deletion of the acidic ^{41}DEWEEE^{46} region (i) weakens but does not abolish Arp2/3 binding, (ii) enhances actin binding, and (iii) allows somewhat reduced bacterial motility may explain why the [120−612] fragment of ActA still activates Arp2/3-induced actin polymerization (*31*).

The binding of PIP2 to ActA inhibits the activation of Arp2/3, with a K_d of about 10 μM, by disrupting the ActA−Arp2/3 interaction. The relatively low affinity of PIP2 for ActA contrasts with the very efficient activation of N-WASp

by PIP2 [$K_d = 0.1$ μM (Carlier, unpublished material)] and raises questions concerning a physiological role of this process.

Like VCA−actin complex (and like profilin−actin), the 1:1 ActA-G-actin complex productively associates to barbed ends of actin filaments. This property adds up to the general evidence that ActA mimics VCA in activating filament branching by Arp2/3 and suggests that other activators of Arp2/3 complex might use the same mechanism. In this respect, cortactin has recently been identified as a weak activator of Arp2/3 complex (*47*, *48*). Cortactin has not been reported to interact with G-actin however, although a putative G-actin binding consensus sequence (TLKEKELET) is found in cortactin.

Our estimate of the actin:ActA molar ratio in the complex differs from Zalevsky et al. (*31*), who analyzed the curves of inhibition of pointed end growth by ActA (like in Figure 4a) within binding of 2 G-actin molecules to ActA. Their analysis erroneously assumes that the rate of pointed end growth is zero when all actin is in complex with ActA. In fact, the rate of pointed end growth is zero when the concentration of free G-actin equals the critical concentration at the pointed end ($C_C^p = 0.6$ μM), as expressed here in eq 3, used to fit data in Figure 4a. In ref *31*, the stoichiometric line representing the formation of a high affinity ActA−actin 1:1 complex therefore should be drawn so as to intercept the concentration axis at an ActA concentration equal to $[\text{G-actin}]_{total} - C_C^p$, instead of $[\text{G-actin}]_{total}$. In this analysis, no room is left in Zalevsky's data for suspecting binding of a second G-actin to ActA.

ActA-activated Arp2/3 complex initiates filament barbed end branching like VCA-activated Arp2/3 complex (*23*). Two experiments rule out side branching: first, barbed end capped filaments fail to activate branching; second, a quantitative analysis of the fluorescence microscopy images of red and green filaments (Figure 5) shows no evidence for side branching. We propose that in the activated ActA-Arp2/3-G-actin ternary complex, the ability of the ActA-bound G-actin to associate with a filament barbed end is part of the barbed end branching activity, and allows the proper positioning of the activated complex and the initiation of the daughter branch from the barbed end of the mother branch. The view that Arp2/3 complex branches filaments from their sides (*24*) has been derived from assays in which (in contrast to ours) phalloidin was present from time zero of the polymerization process, thus biasing the experiment. This bias is likely to be responsible for the absence of length correlation of the mother and daughter branches. If Arp2/3 complex branched filaments from the sides of filaments during polymerization, a length correlation coefficient of 0.65 would be expected. The measured value (0.02−0.04) is in contradiction with the proposed side branching model.

As previously observed with VCA-activated Arp2/3 (*22*, *43*), filament branching by ActA-activated Arp2/3 is followed by debranching. Debranching occurs a short time following branching, so that it is only when the rate of polymerization is fast enough that a high percentage of branched filaments (70%) can be observed as intermediates in the early times of polymerization. The hydrolysis of ATP associated with actin polymerization has been evoked as a plausible explanation for debranching (*43*). However, the rate of debranching is 3-fold higher when ActA rather than the VCA domain of N-WASp is the activator of Arp2/3 and in both cases debranching is slower than Pi release on F-actin; second, Pi and BeF_3^-, which stabilize the F-ADP-Pi state of F-actin, fail to prevent debranching. Hence, in our view, debranching is not likely associated with Pi release on F-actin. Another yet unexplored possibility is that ATP would be hydrolyzed on Arp2 and/or Arp3 upon branching, and this reaction, which might take place at a rate depending on the nature of the activator of Arp2/3, ActA, or VCA, would trigger debranching. An ATPase cycle involved in the branching-debranching activity of Arp2/3 complex might have to be considered.

We propose the following mechanism for spatially controlled actin assembly at the surface of *Listeria*. In the motility medium, MgATP-G-actin is maintained at a high steady-state concentration (about 2 μM) by the actions of capping proteins and actin depolymerizing factor. At this concentration, barbed end nuclei form spontaneously and either abort when they are capped by a capping protein or branch when they interact with ActA-activated Arp2/3 and G-actin at the surface of *Listeria*. Cycles of barbed end growth interrupted by capping or branching generate a branched meshwork at the surface of *Listeria*, Arp2/3 complex remaining located at the short-lived branches. The rate of propulsion and the mesh size are controlled by the balance between Arp2/3 and capping proteins. Recent EM observations of a branched filament network initiated by ActA-coated beads fully support the conclusions of our study (*49*).

The present work rules out a few among the possible roles of VASP in *Listeria* motility, but the issue of the mechanism of VASP remains open. VASP causes a 10-fold increase in the rate of *Listeria* propulsion in the reconstituted motility medium (*25*). During *Listeria* movement, VASP remains tightly bound to ActA at the bacterial surface (*37*, *30*), while Arp2/3 is incorporated in the actin tail (*4*). Here we show that in solution VASP does not bind Arp2/3 complex and does not affect the filament branching/debranching processes, suggesting that it binds ActA independently of Arp2/3. The capping of barbed ends, a reaction which is expected to modulate the rate of propulsion, is not affected by VASP. The fact that ActA-coated beads lose connection with the actin meshwork in the absence of VASP supports the view that VASP is involved in the transient attachment of branched filaments to the surface (*38*). The solution studies done so far with actin, ActA, Arp2/3, and VASP, therefore, suggest that a nonidentified biochemical process, in which VASP is involved, is crucial for movement. Further work is required to understand the molecular details of VASP function.

ACKNOWLEDGMENT

We are grateful to Laurent Blanchoin for advice in fluorescence microscopy observation of branched filaments, to Sophie Cribier for teachnig us how to prepare liposomes, and to Sebastian Wiesner for help with the preparation of ActA-coated beads. E. G., P. D., and P. C. thank Véronique Villiers and Hafida Fsihi for help in constructing the ActA-N mutants.

REFERENCES

1. Beckerle, M. C. (1998) Spatial control of actin filament assembly: Lessons from Listeria. *Cell 95*, 741−748.
2. Cossart, P., and Bierne, H. (2001) The use of host cell machinery in the pathogenesis of Listeria monocytogenes. *Curr. Opin. Immunol. 13*, 96−103.
3. Cameron, L. A., Giardini, P. A., Soo, F. S., and Theriot, J. A. (2001) *Nature Mol. Biol. Rev.* (in press).
4. Welch, M. D., Iwamatsu, A., and Mitchison, T. J. (1997) Actin polymerization is induced by Arp2/3 complex at the surface of *Listeria monocytogenes*. *Nature 385*, 265−269.
5. Welch, M. D., Rosenblatt, J., Skoble, J., Portnoy, D. A., and Mitchison, T. J. (1998) Interaction of Arp2/3 complex and the *Listeria monocytogenes* ActA protein in actin filament nucleation. *Science 281*, 105−108.
6. Winter, D., Podtelejnikov, A. V., Mann, M., and Li, R. (1997) The complex containing actin-related proteins Arp2 and Arp3 is required for the motility and integrity of yeast actin patches. *Curr. Biol. 7*, 519−529.
7. Svitkina, T. M., and Borisy, G. G. (1999) Arp2/3 complex and actin depolymerizing factor/cofilin in dendritic organization and treadmilling of actin filament array in lamellipodia. *J. Cell Biol. 145*, 1009−1026.
8. Rohatgi, R., Ma, L., Miki, H., Lopez, M., Kirchhausen, T., Takenawa, T., and Kirschner, M. W. (1999) The interaction between N-WASP and the Arp2/3 complex links Cdc42-dependent signals to actin assembly. *Cell 97*, 221−331.
9. Kalman, D., Weiner, O. D., Goosney, D. L., Sedat, J. W., Finlay, B. B., Abo, A., and Bishop, J. M. (1999) Enteropathogenic *E. coli* acts through WASP and Arp2/3 complex to form actin pedestals. *Nat. Cell Biol. 1*, 389−391.
10. May, R. C., Caron, E., Hall, A., and Machesky, L. M (2000) Involvement of the Arp2/3 complex in phagocytosis mediated by FcgammaR or CR3. *Nat. Cell Biol. 2*, 246−248.
11. Taunton, J., Rowning, B. A., Coughlin, M. L., Wu, M., Moon, R. T., Mitchison, T. J., and Larabell, C. A (2000) Actin-dependent propulsion of endosomes and lysosomes by recruitment of N-WASP. *J. Cell. Biol. 148*, 519−530.
12. Goldberg D. J., Foley, M. S., Tang, D., and Grabham, P. W. (2000) Recruitment of the Arp2/3 complex and mena for the stimulation of actin polymerization in growth cones by nerve growth factor. *J. Neurosci. Res. 60*, 458−467.
13. Rozelle, A. L., Machesky, L. M., Yamamoto, M., Driessens, M. H., Insall, R. H., Roth, M. G., Luby-Phelps, K., Marriott, G., Hall, A., and Yin, H. L. (2000) Phosphatidylinositol 4,5-bisphosphate induces actin-based movement of raft-enriched vesicles through WASP−Arp2/3. *Curr. Biol. 10*, 311−320.
14. Machesky, L. M., and Insall, R. H. (1998) Scar1 and the related Wiskott-Aldrich syndrome protein, WASP, regulate the actin cytoskeleton through the Arp2/3 complex. *Curr Biol. 8*, 1347−1356.
15. Machesky, L. M., Mullins, R. D., Higgs, H. N., Kaiser, D. A., Blanchoin, L., May, R. C., Hall, M. E., and Pollard, T. D. (1999) Scar, a WASp-related protein, activates nucleation of actin filaments by the Arp2/3 complex. *Proc. Natl. Acad. Sci. U.S.A. 96*, 3739−3744.
16. Egile, C., Loisel, T. P., Laurent, V., Li, R., Pantaloni, D., Sansonetti, P. J., and Carlier, M. F. (1999) Activation of the CDC42 effector N-WASP by the *Shigella flexneri* IcsA protein promotes actin nucleation by Arp2/3 complex and bacterial actin-based motility. *J. Cell Biol. 146*, 1319−1332.
17. Frischknecht, F., Moreau, V., Rottger, S., Gonfloni, S., Reckmann, I., Superti-Furga, G., and Way, M. (1999) Actin-based motility of vaccinia virus mimics receptor tyrosine kinase signalling. *Nature 401*, 926−929.
18. Kim, A. S., Kakalis, L. T., Abdul-Manan, N., Liu, G. A., and Rosen, M. K. (1999) Autoinhibition and activation mechanisms of the Wiskott-Aldrich syndrome protein. *Nature 404*, 151−158.
19. Prehoda, K. E., Scott, J. A., Mullins, R. D., and Lim, W. A. (2000) Integration of multiple signals through cooperative regulation of the N-WASP-Arp2/3 complex. *Science 290*, 80−806.
20. Higgs, H. N., Blanchoin, L., and Pollard, T. D (1999) Influence of the C-terminus of Wiskott-Aldrich Syndrome protein (WASp) and the Arp2/3 complex on actin polymerization. *Biochemistry 38*, 15212−15222.
21. Higgs, H. N., and Pollard, T. D. (1999) Regulation of actin polymerization by Arp2/3 complex and WASp/Scar proteins. *J. Biol. Chem. 274*, 32531−32534.
22. Blanchoin, L., Amann, K. J., Higgs, H. N., Marchand, J. B., Kaiser, D. A., and Pollard, T. D. (2000) Direct observation of dendritic actin filament networks nucleated by Arp2/3 complex and WASP/Scar proteins. *Nature 404*, 1007−1011.
23. Pantaloni, D., Boujemaa, R., Didry, D., Gounon, P., and Carlier, M. F. (2000) The Arp2/3 complex branches filament barbed ends: functional antagonism with capping proteins. *Nat. Cell Biol. 2*, 385−391.
24. Amann, K. J., and Pollard, T. D. (2001) The Arp2/3 complex nucleates actin filament branches from the sides of pre-existing filaments. *Nat. Cell. Biol. 3*, 306−310.
25. Loisel, T. P., Boujemaa, R., Pantaloni, D., and Carlier, M.-F. (1999). Reconstitution of actin-based motility of Listeria and Shigella using pure proteins. *Nature 401*, 613−616.
26. Gertler, F. B., Niebuhr, K., Reinhard, M., Wehland, J., and Soriano, P. (1996) Mena, a relative of VASP and Drosophila Enabled, is implicated in the control of microfilament dynamics. *Cell 87*, 227−239.
27. Rottner, K., Behrendt, B., Small, J. V., and Wehland, J. (1999) VASP dynamics during lamellipodia protrusion. *Nat. Cell Biol. 1*, 321−322.
28. Skoble, J., Portnoy, D. A., and Welch, M. D. (2000) Three regions within ActA promote Arp2/3 complex-mediated actin nucleation and *Listeria monocytogenes* motility. *J. Cell. Biol. 150*, 527−537.
29. Cicchetti, G., Maurer, P., Wagener, P., and Kocks, C. (1999) Actin and phosphoinositide binding by the ActA protein of the bacterial pathogen *Listeria monocytogenes*. *J. Biol. Chem. 274*, 33616−33626.
30. Lasa, I., Gouin, E., Goethals, M., Vankompernolle, K., David, V., Vandekerckhove, J., and Cossart, P. (1997) Identification of two regions in the N-terminal domain of ActA involved in the actin comet tail formation by *Listeria monocytogenes. EMBO J. 16*, 1531−1540.
31. Zalevsky, J., Grigorova, I., and Mullins, R. D. (2001) Activation of the Arp2/3 Complex by the Listeria ActA Protein. ActA binds two actin monomers and three subunits of the Arp2/3 complex. *J. Biol. Chem. 276*, 3468−3475.
32. David, V., Gouin, E., Van Troys, M., Grogan, A., Segal, A., Ampe, C., and Cossart, P. (1998) Identification of cofilin, coronin, Rac and capZ in actin tails using a *L. monocytogenes* affinity approach. *J. Cell Sci. 111*, 2877−2884.
33. Mathivet, L., Cribier, S., and Devaux, P. F. (1996) Shape change and physical properties of giant phospholipid vesicles prepared in the presence of an AC electric field. *Biophys. J. 70*, 1112−1121.
34. Kocks, C., Gouin, E., Tabouret, M., Berche, P., Ohayon, H., and Cossart, P. (1992) *Listeria monocytogenes*-induced actin assembly requires the *actA* gene product, a surface protein. *Cell 68*, 521−531.
35. Smith, K., and Youngmann, P. (1992) Use of a new intergrative vector to investigate compartment-specific expression of the *Bacillus subtilis* spoIIM gene. *Biochimie 74*, 705−711.
36. Camili, A., Tilney, L., and Portnoy, D. (1993) Dual roles of plcA in *L. monocytogenes* pathogenesis. *Mol. Microbiol. 8*, 143−157.
37. Steffen, P., Schafer, D. A., David, V., Gouin, E., Cooper, J. A., and Cossart, P. (2000) *Listeria monocytogenes* ActA protein interacts with phosphatidylinositol 4,5-bisphosphate *in vitro*. *Cell Motil. Cytoskeleton. 45*, 58−66.
38. Laurent, V., Loisel, T. P., Harbeck, B., Wehman, A., Grobe, L., Jockusch, B. M., Wehland, J., Gertler, F. B., and Carlier, M. F (1999) Role of proteins of the Ena/VASP family in actin-based motility of *Listeria monocytogenes*. *J Cell Biol. 144*, 1245−1258.
39. Casella, J. F., Maack, D. J., and Lin, S. (1986) Purification and initial characterization of a protein from skeletal muscle

that caps the barbed ends of actin filaments. *J. Biol. Chem. 261*, 10915−10921.
40. Pistor, S., Gröbe, L., Sechi, A. S., Domann, E., Gerstel, B., Machesky, L. M., Chakraborty, T., and Wehland, J. (2000) Mutations of arginine residues within the 146-KKRRK-150 motif of the ActA protein of *Listeria monocytogenes* abolish intracellular motility by interfering with the recruitment of the Arp2/3 complex. *J. Cell Sci. 113*, 3277−3287.
41. Kocks, C., Marchand, J. B., Gouin, E., d'Hauteville, H., Sansonetti, P. J., Carlier, M.-F., and Cossart P. (1995) The unrelated surface proteins ActA of *Listeria monocytogenes* and IcsA of *Shigella flexneri* are sufficient to confer actin-based motility on Listeria innocua and *Escherichia coli* respectively. *Mol Microbiol. 18*, 413−423.
42. Carlier, M.-F., and Pantaloni, D. (1986) Direct evidence for ADP-Pi-F-actin as the major intermediate in ATP-actin polymerization. Rate of dissociation of Pi from actin filaments. *Biochemistry 25*, 7789−7792.
43. Blanchoin, L., Pollard, T. D., and Mullins, R. D. (2000) Interactions of ADF/cofilin, Arp2/3 complex, capping protein and profilin in remodeling of branched actin filament networks. *Curr. Biol. 10*, 1273−82.
44. Smith, G. A., Theriot, J. H. A., and Portnoy, D. A. (1996) The tandem repeat domain in the *Listeria monocytogenes* ActA protein controls the rate of actin-based motility, the percentage of moving bacteria and the localization of vasodilator-stimulated phosphoprotein and profilin. *J. Cell Biol. 135*, 647−660.
45. Cameron, L. A., Footer, M. J., Van Oudenaarden, A., and Theriot, J. A. (1999) Motility of ActA protein-coated microspheres driven by actin polymerization. *Proc. Nat. Acad. Sci. U.S.A. 96*, 4908−4913.
46. Van Oudenaarden A., and Theriot, J. A. (1999) Cooperative symmetry-breaking by actin polymerization in a model for cell motility. *Nat. Cell Biol. 1*, 493−499.
47. Uruno, T., Liu, J., Zhang, P., Fan, Y.-X., Egile, C., Li, R., Mueller, S. C., and Zhan, X. (2001) Activation of Arp2/3 complex-mediated actin polymerization by cortactin. *Nat. Cell Biol. 3*, 259−266.
48. Weaver, A. M., Karginov, A. V., Kinley, A. W., Weed, S. A., Li, Y., Parsons, T., and Cooper, J. A. (2001) Cortactin promotes and stabilizes Arp2/3-induced actin filament network formation. *Curr. Biol. 11*, 370−374.
49. Cameron, L. A., Svitkina, T. M., Vignjevic, D., Theriot, J. A., and Borisy, G. G. (2001) Dendritic organization of actin comet tails. *Curr. Biol. 11*, 130−135.

BI010486B